Fluorescence during Doppler cooling of a single trapped atom

J. H. Wesenberg,* R. J. Epstein,† D. Leibfried, R. B. Blakestad, J. Britton, J. P. Home, W. M. Itano, J. D. Jost, E. Knill, C. Langer,‡ R. Ozeri,§ S. Seidelin,‖ and D. J. Wineland
National Institute of Standards and Technology, Boulder, Colorado 80305, USA
(Received 9 July 2007; published 26 November 2007)

We investigate the temporal dynamics of Doppler cooling of an initially hot single trapped atom in the weak-binding regime using a semiclassical approach. We develop an analytical model for the simplest case of a single vibrational mode for a harmonic trap, and show how this model allows us to estimate the initial energy of the trapped particle by observing the time-dependent fluorescence during the cooling process. The experimental implementation of this temperature measurement provides a way to measure atom heating rates by observing the temperature rise in the absence of cooling. This method is technically relatively simple compared to conventional sideband detection methods, and the two methods are in reasonable agreement. We also discuss the effects of rf micromotion, relevant for a trapped atomic ion, and the effect of coupling between the vibrational modes on the cooling dynamics.

DOI: 10.1103/PhysRevA.76.053416 PACS number(s): 32.80.Lg, 32.80.Pj, 42.50.Vk

I. INTRODUCTION

Laser cooling of trapped neutral atoms and atomic ions is a well-established technique: for example, cooling to the motional ground state [1–3] and motional state tomography [4] are routinely performed with resolved motional-sideband excitation techniques. Sideband techniques require the natural linewidth Γ of the cooling transition to be small compared to the vibrational frequency of the trapped particle, in order to allow the motional sidebands to be resolved. Many experiments are, however, conducted in the "weak-binding regime," where Γ is larger than the oscillation frequency. Here, the cooling process is essentially the same as Doppler cooling of free atoms, because the spontaneous decay process is short compared to the atom's oscillation period [5]. Even in experimental setups that implement sideband techniques, an initial stage of such "Doppler cooling" is often employed. The first examinations of Doppler cooling of trapped ions [5–11] did not take into account the effects of micromotion due to the trapping rf field. After cooling and heating effects related to micromotion were observed, these effects were explained theoretically [12–14] by including the effects of micromotion.

Here, we consider Doppler cooling of a single trapped atom or ion. While most previous work has focused on the final stages of cooling, our focus will be on the temporal dynamics of the cooling, particularly in the "hot regime" where the Doppler shift due to atom motion is comparable to or much larger than Γ. For the one-dimensional (1D) case we find that the cooling rate can be calculated analytically in the weak-binding regime without assuming the atom to be in the Lamb-Dicke regime. For a trapped ion, when we take rf micromotion into consideration, stable, highly excited states emerge when only one mode is considered [15]. When all three vibrational modes of the ion are considered, we find that couplings between the modes tend to break the stability of such points, allowing cooling to reach the Doppler limit.

A practical application of our results is to estimate the initial motional energy of an atom or ion from observations of the time dependence of the fluorescence during the cooling process. As mentioned above, sideband spectroscopy is the conventional technique for characterizing motional states, and it has been used to characterize the heating rate of ions in the absence of cooling [1,2,16–20]. However, it is more complicated to implement experimentally than Doppler cooling, requiring more laser beams. Currently, considerable effort is being devoted to understanding the heating observed in ion traps [16–20]. This heating is anomalous in that it is typically much higher than would be expected from thermal electronic noise (Johnson noise) that results from resistance associated with the trap electrodes. Because of its pervasive nature and detrimental effects to quantum state manipulation, it is important to understand and eliminate its cause. A less complicated technique for measuring temperature could simplify this work.

We note that cooling of a single ion is significantly different than cooling a large number of ions in the same trap where the degrees of freedom are strongly mixed. However, the cooling and heating of a single ion is interesting because heating can only arise from external fields, not from the effects of ion-ion collisions that can lead to heating for two or more ions [21].

This paper is structured as follows. In Sec. II we present a semiclassical model of the Doppler cooling process for a bound atom confined in one dimension in the weak-binding regime in a static harmonic well (no micromotion). In Secs. III and IV we analyze the fluorescence vs time predicted by the model. Here, we consider single cooling trajectories and average over these with a given distribution of initial motional energies. We derive expressions useful for estimating initial temperature from fluorescence observations in these sections. Section V discusses how to minimize the total measurement time required to estimate the mean initial energy.

*janus.wesenberg@nist.gov
†Present address: Areté Associates, Longmont, CO 80501, USA.
‡Present address: Lockheed Martin, Huntsville, AL, USA.
§Present address: Weizmann Institute of Science, Rehovot, Israel.
‖Present address: Institut Néel, Grenoble, France.

In Sec. VI we consider the effects of other motional modes with and without taking into account any rf micromotion experienced by such modes. The primary result of this section is most relevant for ions confined in miniature linear Paul traps [22,23]. In these traps, ions are bound along the axis by a static harmonic well. In the transverse direction, ions are bound by a ponderomotive pseudopotential where the ions' motion must also include the effects of rf micromotion. Typically, these traps are operated under conditions where the ions' oscillation frequencies in the transverse direction are much higher than along the axis. Moreover, it is typically observed that the anomalous heating as a function of oscillation frequency ω drops off as $1/\omega$ or faster. Therefore, to a good approximation the ion heating is dominated by that along the axis of the trap. In this case the results of Secs. II–IV will be valid to a good approximation. These conclusions are supported by a more complete solution of the problem described in Sec. VI C. Section VII suggests possible modifications to the basic experimental protocol that might provide improved sensitivity of the temperature measurements. Section VIII concludes the paper.

II. MODEL

We consider a semiclassical model of Doppler cooling of a single weakly trapped atom [5,11]. We will initially consider only a single mode of motion, taken to be along the z direction. We assume a harmonic potential with oscillation frequency ω_z. In Sec. VI we consider a more detailed model that includes three dimensions and micromotion relevant for trapped ions.

The atom is Doppler cooled by a single laser beam of angular frequency ν_{laser} and wave vector $\boldsymbol{k}$, detuned by $\Delta \equiv \nu_{\text{laser}} - \nu_{ge}$ from the resonance frequency ν_{ge} of a two-level, or "cycling," transition between two internal states $|g\rangle$ and $|e\rangle$, of the atom. We write the coupling Hamiltonian as

$$H^{(c)} = \hbar\Omega_{\text{Rabi}}(|e\rangle\langle g| + |g\rangle\langle e|)\cos(\boldsymbol{k}\cdot\boldsymbol{x} - \nu_{\text{laser}}t), \tag{1}$$

where $\boldsymbol{x}$ is the atom position, $2\pi\hbar$ is Planck's constant, and Ω_{Rabi} is the resonant Rabi frequency.

We assume the atom is weakly bound in the z direction, that is, ω_z is much smaller than the excited state decay rate Γ. The atom's level populations are then approximately in steady state with respect to the instantaneous effective detuning $\Delta_{\text{eff}} \equiv \Delta + \Delta_D$, including the Doppler shift $\Delta_D \equiv -k_z v_z$, where v_z and k_z are the z components of the velocity and wave vector. The excited state population is then [24]

$$\rho_{ee}(v_z) = \frac{s/2}{1 + s + (2\Delta_{\text{eff}}/\Gamma)^2}. \tag{2}$$

Here s is the saturation parameter, proportional to the cooling beam intensity, $s \equiv 2|\Omega_{\text{Rabi}}|^2/\Gamma^2$.

The excited state population is associated with the photon scattering rate dN/dt by the relation $dN/dt = \Gamma\rho_{ee}(v_z)$. While the momentum kicks associated with photon emission are assumed to average to zero over many absorption-emission cycles, the absorbed photons will impart a velocity-dependent momentum transfer due to the scattering that can be described by a velocity-dependent force

$$F_z(v_z) = m\frac{dv_z}{dt} = \hbar k_z \Gamma \rho_{ee}(v_z), \tag{3}$$

where m is the atom's mass. This velocity-dependent force will in general change the motional energy E of the atom. If the relative change in energy over a motional cycle is small, we can average the effect of F_z over the oscillatory motion to find the evolution of E:

$$\frac{dE}{dt} = \langle v_z F_z(v_z)\rangle, \tag{4}$$

where the average is over one motional cycle. The average energy change per scattering event is $dE/dN = \hbar k_z v_z = -\hbar\Delta_D$.

In addition to F_z, the atom will experience a stochastic force due to photon recoil that, assuming isotropic emission, will cause heating at a rate [11]

$$\left(\frac{dE}{dt}\right)_{\text{recoil}} = \frac{4}{3}\frac{(\hbar k_z)^2}{2m}\frac{dN}{dt}, \tag{5}$$

where $(\hbar k_z)^2/2m$ is the recoil energy associated with the scattering. We will mostly ignore the effects of recoil heating in what follows, since it will be important only near the cooling limit.

III. ANALYSIS

We will now analyze the time dependence of the atom fluorescence during the Doppler cooling process, as predicted by the model introduced above.

To simplify the algebra, we will scale energies by $\hbar$ times half the power-broadened linewidth, and time by the resonant scattering rate:

$$\varepsilon = E/E_0, \quad E_0 = \frac{\hbar\Gamma}{2}\sqrt{1+s}, \tag{6a}$$

$$\delta = \hbar\Delta/E_0, \tag{6b}$$

$$r = \frac{(\hbar k_z)^2}{2m}\Big/ E_0, \tag{6c}$$

$$\tau = t/t_0, \quad t_0 = \left(\Gamma\frac{s/2}{1+s}\right)^{-1}. \tag{6d}$$

As an example of typical values, we consider a trapped $^{25}Mg^+$ ion, where the $^2S_{1/2}$-$^2P_{3/2}$ cooling transition at 279.6 nm has a natural linewidth of $\Gamma = 2\pi\times 41.4$ MHz. At a detuning of $\Delta = -2\pi\times 20$ MHz with $s=0.9$ and $k_z/k = 0.71$, we find that $E_0/k_B = 1.4$ mK, where k_B is Boltzmann's constant and $t_0 = 16$ ns. The detuning and recoil parameters are $\delta = -0.70$ and $r = 0.0018$.

For a given motional energy ε, the instantaneous Doppler shift $\delta_D \equiv \hbar\Delta_D/E_0$ has a maximal value of $\delta_M \equiv 2\sqrt{\varepsilon r}$. In the scaled units, the average change in energy per scattering event is $-\delta_D$, so δ_M is also equal to the maximal change in energy per scattering event. As explained below, the energy at which the maximal Doppler shift is equal to the power-

broadened linewidth, $\varepsilon = 1/r$, is of interest during the cooling process. For reference we note that this energy corresponds to

$$\frac{1}{r}E_0 = (1+s)\frac{\hbar^2\Gamma^2}{4}\frac{2m}{\hbar^2 k_z^2}. \tag{7}$$

For the typical experimental parameters considered above, E_0/r is equal to $k_B \times 0.7$ K or 3700 $\hbar\omega_z$ for $\omega_z = 2\pi \times 4.0$ MHz.

For harmonic oscillations, the instantaneous Doppler shift δ_D is distributed according to the probability density

$$P_D(\delta_M;\delta_D) = \int_0^{2\pi} \delta_{\text{Dirac}}[\delta_D - \delta_M \sin(\phi)]\frac{d\phi}{2\pi} = \begin{cases} \frac{1}{\pi}\frac{1}{\sqrt{\delta_M^2 - \delta_D^2}} & \text{if } |\delta_D| < \delta_M, \\ 0 & \text{otherwise,} \end{cases} \tag{8}$$

where δ_{Dirac} is the Dirac δ function. Examples of this probability distribution for two different values of δ_M are shown in the insets of Fig. 1. Since the average energy change per scattering event is $-\delta_D$, and the instantaneous scattering rate is $1/(1+\delta_{\text{eff}}^2)$, where $\delta_{\text{eff}} \equiv \delta + \delta_D$, the rate of change of ε averaged over the secular oscillations, given by Eq. (4), takes the form

$$\frac{d\varepsilon}{d\tau} = \int -\delta_D P_D(\delta_M;\delta_D)\frac{1}{1+(\delta+\delta_D)^2}d\delta_D. \tag{9}$$

We can evaluate the integral as detailed in Appendix A, to find that

$$\frac{d\varepsilon}{d\tau} = \frac{1}{2\sqrt{\varepsilon r}}[\text{Re}(Z) + \delta\,\text{Im}(Z)], \tag{10a}$$

$$\approx \frac{\delta}{2\sqrt{\varepsilon r}}, \quad \varepsilon \gg (1+\delta^2)/r, \tag{10b}$$

where $Z = Z(\delta,\delta_M) = i/\sqrt{1-(\delta+i)^2/4\varepsilon r}$. The asymptotic approximation (10b) corresponds to approximating $P_D(\delta_M;\delta_D)$ by $P_D(\delta_M;0)$, which is reasonable in the hot regime, where the peaks of P_D have small overlap with the Lorentzian line profile. From Eqs. (10a) and (10b), we can evaluate ε as a function of time; an example is shown in the lower part of Fig. 1.

The scattering rate averaged over the motion is analogous to Eqs. (10a) and (10b) and is given by

$$\frac{dN}{d\tau} = \int P_D(\delta_M;\delta_D)\frac{1}{1+(\delta+\delta_D)^2}d\delta_D = \frac{1}{2\sqrt{\varepsilon r}}\text{Im}(Z), \tag{11}$$

as illustrated in the upper part of Fig. 1. In the limit of $\varepsilon \gg (1+\delta^2)/r$, we find $dN/d\tau \approx 1/(2\sqrt{\varepsilon r})$, so that according to Eq. (10b) we have in this limit $d\varepsilon/dN \approx \delta$. In physical units, this corresponds to each photon on average extracting an energy of $\hbar\Delta$. This can be understood by noting that, in the limit of $\varepsilon \gg (1+\delta^2)/r$, $P_D(\delta_M;\delta_D)$ is to a good approximation uniform over the Lorentzian line profile (see, for example, the upper left inset of Fig. 1), and so the value of $\delta_{\text{eff}} = \delta + \delta_D$ averaged over the scattering events will be nearly zero. Since each scattering event extracts an energy of $-\delta_D$, the average cooling per scattering event should indeed be δ.

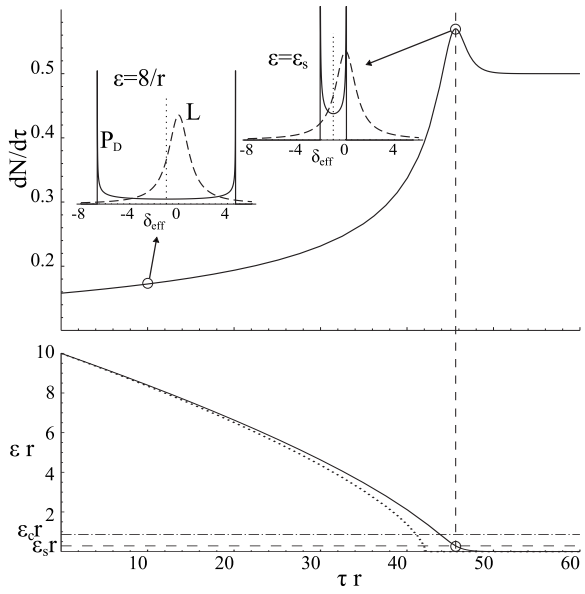

FIG. 1. Scattering rate (top) and energy (bottom) as a function of time during the Doppler cooling of a single atom from an initial energy [in scaled units, see Eq. (6a)] of $10/r$, as given by Eqs. (11), (10a), and (10b), at a detuning of half the power-broadened linewidth [$\delta = -1$; see Eq. (6b)]. The dotted curve in the lower plot shows the energy as a function of time predicted by the asymptotic approximation of Eq. (12). Insets in the upper plot show (at two different times) the two components appearing in the integral defining $dN/d\tau$ in Eq. (11), the probability density of the effective detuning $P_D(\delta_M;\delta_{\text{eff}}-\delta)$ (solid) and the Lorentzian line profile, $L(\delta_{\text{eff}}) = 1/(1+\delta_{\text{eff}}^2)$ (dashed), as functions of $\delta_{\text{eff}} = \delta + \delta_D$ at $\varepsilon = 8/r$ and $\varepsilon = \varepsilon_s$ [Eq. (14)]. Scattering events where the atom is moving toward the laser so that $\delta_D > 0$, corresponding to the rightmost peak of P_D, result in cooling, and vice versa. The energies of maximal cooling and scattering rates, ε_c and ε_s, are given by Eqs. (13) and (14).

The time dependence of ε is formally found by integrating $d\varepsilon/d\tau$ as given by Eqs. (10a) and (10b). For the asymptotic approximation (10b) we find

$$\varepsilon(\tau) \approx \left(\varepsilon_0^{3/2} + \frac{3\delta\tau}{4\sqrt{r}}\right)^{2/3}, \quad \varepsilon \gg (1+\delta^2)/r, \tag{12}$$

where ε_0 is the energy at $\tau = 0$, as plotted in the lower part of Fig. 1. For the exact expression derived from Eq. (10a), we must resort to numerical methods to find $\varepsilon(t)$. Nevertheless, we do find analytically that the cooling rate is maximal for ε related to δ by

$$\varepsilon = \varepsilon_c \equiv \frac{1+\delta^2}{2r}\cos\left[\frac{1}{3}\arccos\left(\frac{1-\delta^2}{1+\delta^2}\right)\right], \tag{13}$$

which quantifies our previous observation that $1/r$ is a typical energy scale of the cooling process.

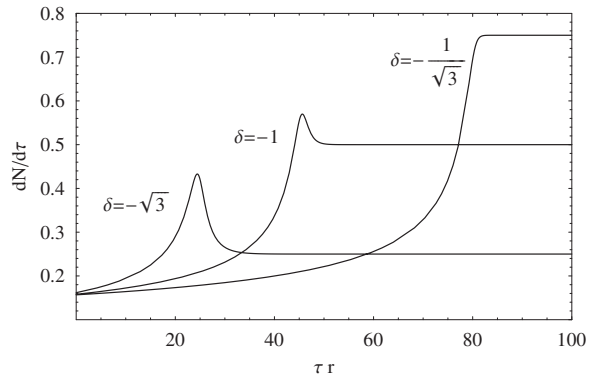

FIG. 2. Scattering rate $dN/d\tau$ vs time during Doppler cooling of a single atom with initial energy $\varepsilon=10/r$ for different laser detunings. For $\delta<\delta_c=-1/\sqrt{3}$, a maximal scattering rate occurs at $\varepsilon=\varepsilon_s$, as given by Eq. (14). The maximal value of the scattering rate is given by Eq. (15). Closer to resonance ($\delta_c<\delta<0$), the scattering rate increases monotonically during the cooling.

The behavior of $dN/d\tau$ is qualitatively different for δ being smaller or larger than a critical detuning $\delta_c\equiv-1/\sqrt{3}$. For $\delta<\delta_c$, $dN/d\tau$ has a maximum at an energy

$$\varepsilon=\varepsilon_s\equiv\frac{1}{4r}(\delta-\sqrt{3})(\delta+1/\sqrt{3}). \tag{14}$$

For the example parameters listed below Eqs. (6a)–(6d), δ_c corresponds to a detuning of $\delta_c E_0/\hbar=-2\pi\times 16.5$ MHz. The maximal scattering rate is reached when one of the peaks of the Doppler distribution (8) is in resonance with the cooling transition, as illustrated in the upper right-hand inset in Fig. 1. In the regime where a maximum exists, the maximal scattering rate is found to exceed the steady state scattering rate by a factor of

$$\left.\frac{dN}{d\tau}\right|_{\varepsilon=\varepsilon_s}\Big/\left.\frac{dN}{d\tau}\right|_{\varepsilon=0}=\frac{\sqrt{3\sqrt{3}}}{4}\frac{1+\delta^2}{\sqrt{|\delta|}}. \tag{15}$$

Closer to resonance, i.e., when $\delta_c<\delta<0$, no maximum occurs, as illustrated in Fig. 2.

We emphasize that the only approximations made above are the weak-binding approximation and the omission of recoil heating. In particular, the trapped particle is not assumed to be in the Lamb-Dicke regime. For the weak-binding regime, $\delta_M>1$ implies that the motion is outside the Lamb-Dicke regime. To find the cooling rate predicted by Eqs. (10a) and (10b) in the Lamb-Dicke limit, we note that to first order in ε we find $d\varepsilon/d\tau\approx 4\delta\varepsilon r/(1+\delta^2)^2$. This corresponds to ε decreasing exponentially with τ. Except for the omission of recoil heating, the value of the decay time agrees with previous work that assumed the atom was in the Lamb-Dicke regime [5,25].

In the above analysis, we have ignored recoil heating [given by Eq. (5)]. In the limit of $\varepsilon\gg\varepsilon_c$, the ratio of heating to cooling is seen to be $4r/(3|\delta|)$, which is a small fraction for typical experimental parameters. For $\varepsilon<\varepsilon_c$, the cooling is less efficient and the contribution from recoil becomes more significant, leading to a nonzero steady-state energy. Nevertheless, ignoring recoil heating is reasonable when observing fluorescence scattering, since the scattering rate has almost reached its steady state value when the effect of recoil becomes important. Therefore we have omitted recoil heating in this analysis to make δ the only free parameter and simplify the discussion. Recoil can be included in calculations by combining Eqs. (5), (10a), and (11).

IV. THERMAL AVERAGING

An application of the analysis presented above is to estimate the initial motional energy of a trapped atom from the time-dependent fluorescence observed during the cooling process. Using this method, we can estimate the average rate of heating experienced by a trapped atom in the absence of cooling by first allowing the atom to heat up without cooling for a certain period and then observing the time dependence of the fluorescence as the atom is recooled. As discussed in Sec. III, when $\varepsilon\gg(1+\delta^2)/r$, the average cooling per scattering event is δ. The approximate total number of photons scattered during the cooling of an atom with initial motional energy $\varepsilon_{\text{initial}}$ can consequently be approximated by $|\varepsilon_{\text{initial}}/\delta|$. For the example parameters given in Sec. III, this corresponds to $\approx$3200 photons for $\varepsilon_{\text{initial}}=4/r$, corresponding to $k_B\times 2.8$ K. With typical photon detection efficiencies of less than 10^{-3}, very few photons are registered in a single experiment. We must therefore repeat many experimental cycles consisting of a heating period and a cooling period.

We now consider the form of the fluorescence signal when averaged over many such experimental cycles. Here, we will assume that the heating is stochastic and take the distribution $P_0(\varepsilon)$ of the motional energies at the beginning of each cooling period to be the Maxwell-Boltzmann distribution with mean energy $\bar{\varepsilon}$,

$$P_0(\varepsilon)=\frac{1}{\bar{\varepsilon}}e^{-\varepsilon/\bar{\varepsilon}}. \tag{16}$$

However, the results below hold for any form of $P_0(\varepsilon)$.

The thermally averaged scattering rate is conveniently written in terms of the propagator Ξ of ε: Let $\Xi(\varepsilon_0,\tau)$ denote the energy at time τ of an atom with initial energy $\varepsilon(\tau=0)=\varepsilon_0$. We can then write the thermally averaged scattering rate at time τ as

$$\left\langle\frac{dN}{d\tau}\right\rangle_{\bar{\varepsilon}}=\int_0^\infty P_0(\varepsilon')\left.\frac{dN}{d\tau}\right|_{\varepsilon=\Xi(\varepsilon',\tau)}d\varepsilon'. \tag{17}$$

This can be efficiently computed numerically by noting that $\Xi(\Xi(\varepsilon,\tau_1),\tau_2)=\Xi(\varepsilon,\tau_1+\tau_2)$, as detailed in Appendix B. Figure 3 shows the thermally averaged scattering rate for a few different parameters.

The fluorescence predicted by Eq. (17) has been found to be in agreement with experimentally observed fluorescence. We show one experimental data set for comparison in Fig. 4; the experiments are more fully described in Ref. [20]. Furthermore, the resulting estimated heating rates have been found to agree reasonably well with results obtained using the Raman sideband technique [17,20]. This agreement may at first seem surprising, given that the two methods probe

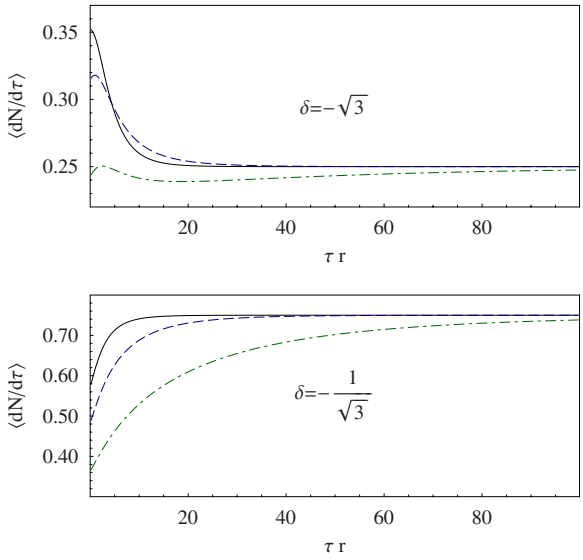

FIG. 3. (Color online) Thermally averaged scattering rate vs time, for $\delta=-\sqrt{3}$ (top) and $-1/\sqrt{3}=\delta_c$ (bottom). In both figures, P_0 is assumed to be a thermal distribution [Eq. (16)] with $\bar{\varepsilon}$ equal to one, two, and four times ε_c for the solid, dashed, and dash-dotted lines, respectively. Note that, for $\delta<\delta_c=-1/\sqrt{3}$, the initial fluorescence is larger than the steady state fluorescence for low values of $\bar{\varepsilon}$; this is attributed to the local maximum in the fluorescence vs time as illustrated in Fig. 2.

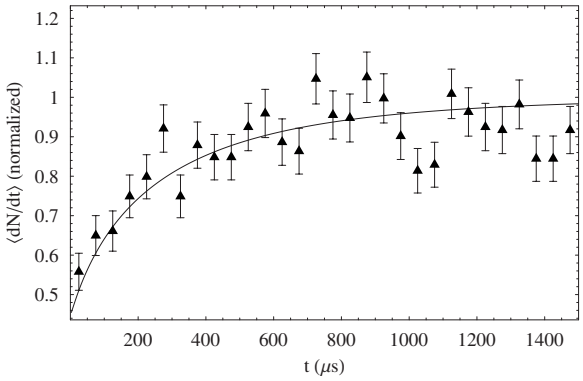

FIG. 4. Experimentally observed fluorescence during Doppler cooling of a single $^{25}Mg^+$ ion [20] compared with the fluorescence predicted by the simple 1D model. Data points (triangles) indicate the observed scattering rates, obtained by integrating over many experiments. In each experiment, the time-resolved fluorescence is recorded during ion recooling, after the ion has been allowed to heat up for a period of 25 s. The experimental parameters are those given after Eqs. (6a)–(6d). Error bars are based on counting statistics. The solid curve is the scattering rate predicted by Eq. (17), assuming the motional energy of the ion after the heating period to be given by the Maxwell-Boltzmann distribution (16) with $\bar{\varepsilon}=5.1/r$, corresponding to a temperature of 3.9 K. Since $\bar{\varepsilon}$ is the only free parameter of Eq. (17), the estimated value was extracted by a single-parameter fit, and agrees reasonably well with an independent temperature estimate of 3.4 ± 0.3 K extrapolated from heating rates measured in the same trap by use of the Raman sideband technique [20].

very different energy scales and that the Raman sideband technique is not sensitive to collisional heating. For the measurements based on the Raman sideband technique the ion was allowed to heat for only a few milliseconds, thereby gaining a few motional quanta. In contrast, the measurement results presented in Fig. 4 are based on 25 s heating periods, allowing the ion to gain many motional quanta. However, the results should agree if, as is currently believed, the heating rate is dominated by the effects of stochastic field fluctuations originating at the electrodes [16]. In this case, we would not expect any thermalization effects before the ion temperature is comparable to that of the electrodes. We would also not expect the effective temperature of the electrodes to be below the ambient temperature ($\approx$300 K).

V. OPTIMAL EXPERIMENTAL PARAMETERS

We now examine how the total measurement time required to reach a given accuracy in the heating rate estimate depends on the choice of experimental parameters. As the recoil parameter r will be fixed by the choice of atom, we consider only the choice of optimal values for initial ion energy $\bar{\varepsilon}$, cooling laser detuning δ, and saturation parameter s.

The experimental signal during a single recooling cycle will consist of an initial deviation from the steady state scattering rate. For a given initial motional energy, both the size and duration of this deviation increase with decreasing detuning, as illustrated by Fig. 2. For a given experimental setup, the optimal detuning is decided as a compromise between recooling signal and ability to recool atoms that have been highly excited by, e.g., collisions.

For a given value of $\bar{\varepsilon}$, the experimental signal, in terms of the number of photons scattered before steady state is reached, does not depend on the laser beam intensity. Since $\bar{\varepsilon}$ is the average initial energy relative to E_0, which is proportional to the power-broadened linewidth, a lower laser beam intensity will give a larger signal for a given heating period. This suggests using the smallest feasible laser intensity, requiring a compromise with respect to robust cooling and detector dark counts. From this standpoint we want to keep the saturation parameter below, but probably close to, 1.

For a given detuning and laser intensity, an additional choice of the length of the heating period in each experimental cycle has to be made: Should we perform a relatively low number of cycles with long heating periods or more cycles with shorter heating periods? To answer this question, we estimate the total measurement time T_{tot} required to reach a certain relative accuracy in the estimate of the heating rate. We assume a constant heating rate and assume that the total time is dominated by the heating periods, so that T_{tot} is proportional to the average initial energy $\bar{E}\propto\bar{\varepsilon}\sqrt{1+s}$, and to the number of runs.

We consider a setup where the observed fluorescence is collected in sequential time bins that are short compared to the total time required for the cooling process. In the limit where the distribution of the integrated number of counts n_i in time bin i is described by a normal distribution with vari-

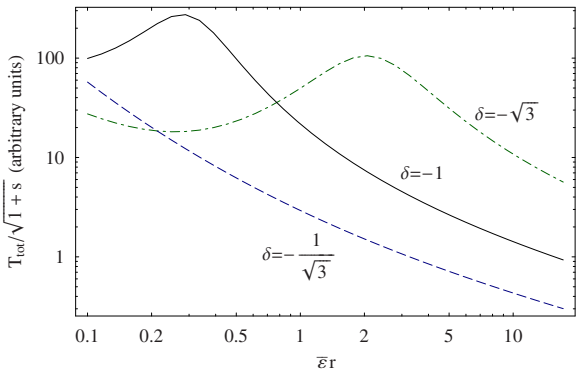

FIG. 5. (Color online) Total measurement time required to establish the heating rate with a given accuracy, assuming this time is dominated by time for reheating. A local maximum is observed for all detunings, but for $\delta=-1/\sqrt{3}$ it is located outside the range covered by the plot.

ance σ_i, we can estimate the uncertainty on the maximum-likelihood estimate of $\bar{\varepsilon}$ for a given data set by [26]

$$1/\sigma(\bar{\varepsilon})^2 = \sum_i \left(\frac{\partial n_i}{\partial \bar{\varepsilon}}\right)^2 \Big/ \sigma_i^2. \tag{18}$$

It follows from Eqs. (10a), (11), and (17), that in the 1D case the cooling dynamics can be rewritten in a form independent of r by reparametrizing in terms of Nr, εr, and τr. We will denote the reparametrized scattering rate by

$$\bar{R}_\delta(\bar{\varepsilon}r, \tau r) = \left\langle \frac{\partial(Nr)}{\partial(\tau r)} \right\rangle_{\bar{\varepsilon}r}. \tag{19}$$

Since the relative uncertainty on the heating rate estimate is equal to $\sigma(\bar{\varepsilon})/\bar{\varepsilon}$ and $\sigma_i=\sqrt{n_i}$, Eqs. (18) and (19) allow us to estimate the time required to obtain a given relative uncertainty on the heating rate:

$$\frac{T_{\text{tot}}}{\sqrt{1+s}} \propto \left[\bar{\varepsilon}r \int_0^\infty \left(\frac{\partial \bar{R}_\delta(\bar{\varepsilon}r,q)}{\partial \bar{\varepsilon}r}\right)^2 \frac{dq}{\bar{R}_\delta(\bar{\varepsilon}r,q)}\right]^{-1}. \tag{20}$$

Note that the right-hand side depends only on δ and $\bar{\varepsilon}r$. Figure 5 shows $T_{\text{tot}}/\sqrt{1+s}$ calculated for different detunings. The figure confirms that a low detuning is indeed favorable, and also shows that, for a given detuning, T_{tot} decreases with increasing $\bar{\varepsilon}$. This is not surprising, given that the time to extract a certain amount of energy increases with atom temperature, as illustrated by Fig. 1. From Fig. 5 and the definition of ε_c [Eq. (13)], we can see that the heating period should be chosen long enough to get a significant signal, i.e., $\bar{\varepsilon} > \varepsilon_c$, but the optimal heating period must be decided based on other experimental parameters such as trap depth and background gas collision rate.

VI. COOLING IN THREE DIMENSIONS

So far, we have considered only cooling in one dimension. In this section we will consider the effect of the vibrational modes in other directions on the cooling process. Our goal is to gain a qualitative understanding of the effects of the transverse modes on the cooling dynamics of the z mode, with the intent of establishing to what extent the simple 1D model presented above is a reasonable approximation.

A. 3D cooling of neutral atoms

For a neutral atom, the confinement transverse to z is not associated with micromotion, as it is for ions in a linear Paul trap, and the 1D weak-binding model extends immediately to three dimensions. Following Sec. III, let ε_i, $i=\{x,y,z\}$, denote the motional energy in mode i, $\delta_D^{(i)}=-\hbar k_i v_i/E_0$ the Doppler shift, and $\delta_M^{(i)}=2\sqrt{\varepsilon_i r_i}$ the maximum Doppler shift. Although the cooling of all modes is formally identical in the absence of micromotion, we will discuss the cooling dynamics with a focus on the z mode.

In experiments it is typically easy to make the frequencies of the three modes incommensurate, which we will assume here. In that case, we can write the rate of change of ε_z as

$$\frac{d\varepsilon_z}{d\tau} = \int \frac{-\delta_D^{(z)}}{1+(\delta+\sum_j \delta_D^{(j)})^2} \prod_l P_D(\delta_M^{(l)};\delta_D^{(l)}) d^3\boldsymbol{\delta}_D$$

$$= \int -\delta_D^{(z)} P_D(\delta_M^{(z)};\delta_D^{(z)}) R_z(\delta+\delta_D^{(z)}) d\delta_D^{(z)}, \tag{21}$$

where R_z is the effective line profile experienced by the z mode, obtained by convolving the Lorentzian line profile with the distribution $P_D^{(x,y)}$ of the combined Doppler shift $\delta_D' \equiv \delta_D^{(x)}+\delta_D^{(y)}$ due to the x and y "spectator" modes,

$$P_D^{(x,y)}(\delta_D') = \int P_D(\delta_M^{(x)};u) P_D(\delta_M^{(y)};\delta_D'-u) du. \tag{22}$$

For the 3D case, R_z replaces the Lorentzian factor $1/[1+(\delta+\delta_D)^2]$ of Eq. (9). As illustrated in Figs. 6 and 7(a), $P_D^{(x,y)}$ is peaked (diverges) at $\delta_D'=\pm|\delta_M^{(x)}-\delta_M^{(y)}|$. If $|\delta_M^{(x)}-\delta_M^{(y)}| \gtrsim 2$, the peaks are separated by more than the width of the Lorentzian profile, and R_z will be double peaked, as illustrated by the solid line in Fig. 7(b). It follows from Eq. (21) that the cooling rate in the limit of small $\delta_M^{(z)}$ is proportional to the slope of R_z at δ, and that the rate of change of ε_z is positive if the slope is negative. If $-|\delta_M^{(x)}-\delta_M^{(y)}| < \delta < 0$, this will result in heating of the z mode, at least as long as $\delta \pm \delta_M^{(z)}$ are both inside the peaks of R_z, that is, when $\delta_M^{(z)} < |\delta_M^{(x)}-\delta_M^{(y)}| + \delta$, as illustrated by the solid curve in Fig. 7(c) for $(\delta_M^{(x)},\delta_M^{(y)})=(0,4)$ and (1,3) [13,15]. The figure also shows that this thermalization or energy equilibration effect is not present if $|\delta_M^{(x)}-\delta_M^{(y)}| \lesssim 1$, as R_z is not double peaked in this case. Mathematically, $d\varepsilon_z/dt$, R_z, and $P_D^{(x,y)}$ are all conveniently expressed as convolution integrals of functions with known Fourier transforms.

The dashed lines in Fig. 8 show the cooling rates predicted by Eq. (21) for the case of the x spectator mode excited, for various energies of the two modes. When $\delta_M^{(z)}$ is large compared to $\delta_M^{(x)}$, we see from the right-hand side of Fig. 8(b) that the z cooling rate is almost unaffected by the x spectator mode. This can be understood by noting that, in the

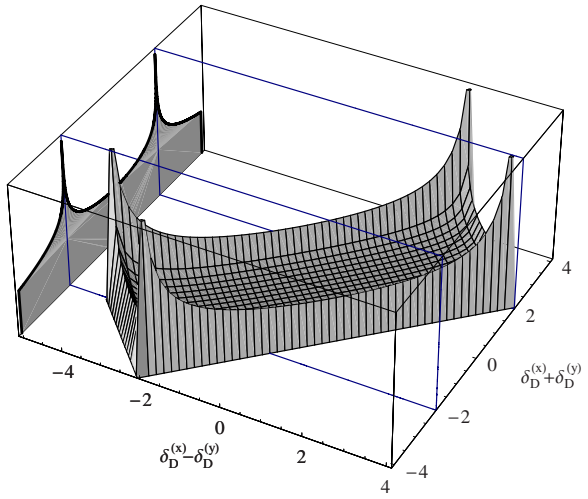

FIG. 6. (Color online) Probability density Eq. (22) for the combined Doppler shift $\delta'_D=\delta_D^{(x)}+\delta_D^{(y)}$ due to two excited modes (curve on left wall) is a marginal distribution of the joint probability density $P_D(\delta_M^{(x)},\delta_D^{(x)})P_D(\delta_M^{(y)},\delta_D^{(y)})$ of $(\delta_D^{(x)},\delta_D^{(y)})$ (3D surface). Note that only two of the peaks in the joint probability distribution lead to peaks in the marginal distribution. Plot is drawn for $\delta_M^{(x)}=3$ and $\delta_M^{(y)}=1$, as the dash-dotted line in Fig. 7(a), and the joint distribution is truncated to $|\delta_D^{(i)}|<0.95\ \delta_M^{(i)}$ for illustrational purposes.

limit where $P_D(\delta_M^{(z)};\delta_D^{(z)})$ is uniform over the values of $\delta_D^{(z)}$ where $R_z(\delta+\delta_D^{(z)})$ is nonzero, the symmetry of R_z implies that the average energy change per scattering event is δ, as also discussed in Sec. III. Since $R_z(\delta_{\text{eff}})\approx 0$ for $\delta_{\text{eff}}>1+\delta_M^{(x)}+\delta_M^{(y)}$, this implies that the temperature of the spectator modes will not affect the cooling rate in this limit. At lower values of $\delta_M^{(z)}$, we generally see a decrease in the cooling rate in a gradual approach to the thermalization regime discussed above.

The consequences of thermalization and equilibration process are complex, when considering the full 3D cooling problem. Consider for instance the case where only one mode is initially hot. According to the discussion above, this will result in heating of the two remaining modes, until the fastest-heating mode has reached a value of δ_M similar to that of the initially hot mode. After this thermalization, the modes will be cooled simultaneously at a cooling rate significantly lower than the cooling rate for a single hot mode.

At this point, it is worth reconsidering the validity of our omission of recoil heating. The recoil heating rate as given by Eq. (5) is seen to have a maximum value of $4r/3$ at the resonant scattering rate. It is clear from Fig. 8 that for typical values of r on the order of 10^{-3}, recoil is insignificant at high energies.

B. 3D cooling of ions including the effects of micromotion

For an ion in a linear Paul trap, if we take the z direction to be the axis, confinement in the transverse x and y directions is provided by the ponderomotive potential of a rf quadrupole field. The full 3D cooling problem including micromotion on the transverse modes is very complex even in

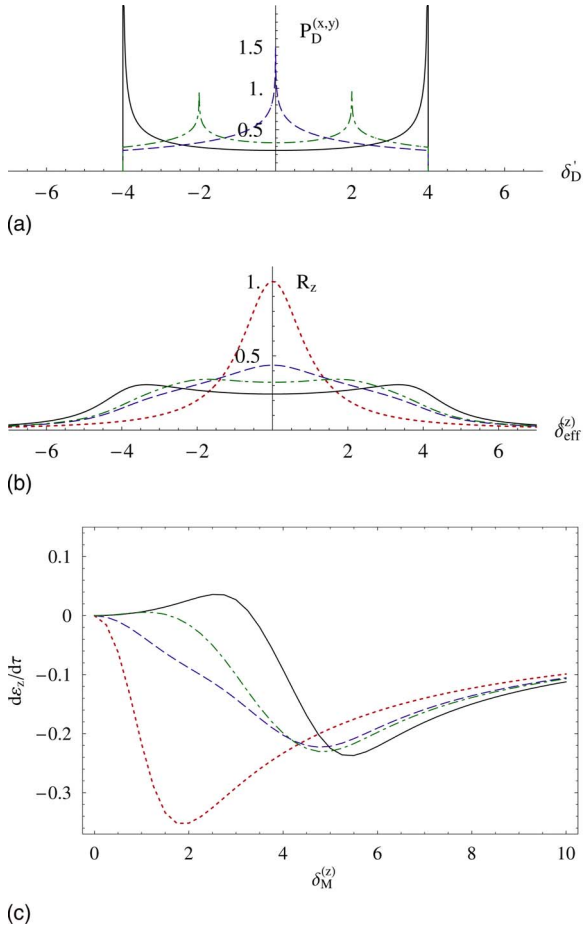

FIG. 7. (Color online) Cooling of the z mode with two excited spectator modes in the absence of micromotion. (a) shows the probability density $P_D^{(x,y)}$ of the combined Doppler shift due to the x and y modes for $(\delta_M^{(x)},\delta_M^{(y)})$ equal to (0,4) (solid), (2,2) (dashed), and (3,1) (dash-dotted). (b) shows the effective line profile $R_z(\delta_{\text{eff}}^{(z)})$ obtained by convolving $P_D^{(x,y)}$ with the Lorentzian line profile. Here $\delta_{\text{eff}}^{(z)}=\delta+\delta_D^{(z)}$. The spectator mode parameters are the same as for (a), and the different curves correspond to the same values of $(\delta_M^{(x)},\delta_M^{(y)})$ as in (a). The dotted line shows the Lorentzian line profile, corresponding to the spectator modes being cold, essentially the 1D cooling case. (c) shows the z mode cooling rate for $\delta=-1$ as a function of $\delta_M^{(z)}$ for the line profiles of (b).

the Lamb-Dicke regime [13,14,21]. At low saturation, the effects of the micromotion caused by a rf field of frequency Ω can be modeled by including micromotion sidebands in the line profile [13]. Micromotion with peak amplitude $\boldsymbol{a}(\bar{\boldsymbol{x}}(t))$, where $\bar{\boldsymbol{x}}$ is the ion position averaged over one period of the rf field, can be described by the line profile

$$R_\mu(\delta_{\text{eff}},\beta)=\sum_{n=-\infty}^{\infty}J_n^2(\beta)\frac{1}{1+(\delta_{\text{eff}}-n\tilde{\Omega})^2},\qquad(23)$$

where $\delta_{\text{eff}}=\delta+\Sigma_j\delta_D^{(j)}$ is the effective detuning, $\beta=|\boldsymbol{a}(\bar{\boldsymbol{x}})\cdot\boldsymbol{k}|$ is the micromotion modulation index, $\tilde{\Omega}=\hbar\Omega/E_0$ is the scaled rf frequency, and J_n is the nth Bessel function.

In contrast to the situation in Ref. [13], we are considering a case where β changes during the secular motion. Since β and δ_{eff} depend on $\bar{\boldsymbol{x}}$ and $\dot{\bar{\boldsymbol{x}}}$, respectively, we parametrize the secular motion by the instantaneous phases ϕ_i, where $\bar{x}_i = \bar{x}_i^{(0)} \cos[\phi_i(t)]$, and where $\bar{x}_i^{(0)}$ is slowly varying and $\dot{\phi}_i \approx \omega_i$. Choosing the x and y axes so that the rf field is proportional to $(\bar{x}\hat{\boldsymbol{x}} - \bar{y}\hat{\boldsymbol{y}})\cos(\Omega t)$, we find that $\delta_D^{(i)} = \delta_M^{(i)} \sin(\phi_i)$. In the limit where the transverse confinement is modified only weakly by static potentials [22,23], so that $\omega_x \approx \omega_y$, we find in the pseudopotential approximation that $\beta = \sqrt{2}|\delta_M^{(x)} \cos(\phi_x) - \delta_M^{(y)} \cos(\phi_y)|/\tilde{\Omega}$, which we note to be independent of the secular frequencies. In this case we have

$$\frac{d\varepsilon_i}{d\tau} = -\int \delta_i R_\mu(\delta_{\text{eff}}(\boldsymbol{\phi}), \beta(\phi_x, \phi_y)) \frac{d^3\boldsymbol{\phi}}{(2\pi)^3}, \tag{24}$$

where the integral is over $[0, 2\pi]$ in all dimensions. Note that, since the modulation index depends only on the transverse components of the motion, the effect of excited transverse modes on the cooling of the z mode can still be described in terms of an effective line profile similar to R_z in Eq. (21).

For the cooling of the transverse modes, the effects of micromotion on the cooling rates are pronounced, as illustrated by the solid curves in Fig. 8(a). A very clear qualitative difference from the cooling rate in the micromotion-free case is that, at sufficiently high rf frequencies ($\tilde{\Omega} > 4.4$ for $\delta = -1$), stable points for the transverse mode energies develop even when the remaining modes are cold. This effect has been discussed in Ref. [15] and is attributed to the heating peak of the Doppler distribution becoming resonant with a micromotion sideband, as described by Eq. (23). This might be related to the bistable behavior reported in some single-ion experiments [21,27,28]. The stability breaks down when thermalization is taken into consideration. Consider, for instance, the stable point indicated in Fig. 8(a) for $\delta_M^{(x)} \approx 7.6$. Here, it is clear from the figure that, when the z mode has heated to $\delta_M^{(z)} > 2$, cooling of the x mode will commence.

When $\delta_M/\tilde{\Omega} \lesssim \sqrt{2}$ for the transverse modes, we find that only the J_0 term of Eq. (23) contributes significantly, and the argument of Sec. VI A that the cooling rate for the z mode is not affected by excited transverse modes when $\delta_M^{(z)} > 1 + \delta_M^{(x)} + \delta_M^{(y)}$ also applies here, as illustrated by Fig. 8(b).

Finally, another effect with respect to micromotion is that the presence of uncontrolled static stray fields can result in the ion experiencing micromotion even at the ion equilibrium position. At temperatures where $\delta_M \ll \tilde{\Omega}$, the first-order effect according to Eq. (23) of this will be a reduction of the central spectral component by a factor of $J_0(\beta)^2$; see, for example, Ref. [29]. We note that this effect can be compensated by using an effective saturation parameter based on the steady state fluorescence observed in the trap.

It is clear from the results in this section that we cannot ignore the transverse modes if their associated maximal Doppler shifts are comparable to that of the z mode. If, however, we assume the transverse modes are cold enough to avoid the heating effects described in Figs. 7 and 8, we have seen above that the primary effect of the transverse modes will be to reduce the cooling rate of the z mode. This would result in the 1D model overestimating the mean initial energy of the z mode. However, for most experiments that use linear rf traps, it is reasonable to assume that the transverse modes are heated significantly less than the z mode. This is because most investigations of the anomalous heating in ion traps have found the results to be consistent with heating rates having a frequency dependence of ω^{-n} with $n > 1$ [16,18,20]. Since the transverse mode frequencies are often an order of magnitude larger than ω_z, this would indeed lead to the transverse modes being significantly colder than the z mode. Also, since the energy in the transverse modes affects only the cooling of the z mode through the resulting Doppler shift, the effect of the transverse modes could be further reduced by arranging $\boldsymbol{k}$ to have a smaller projection on the transverse

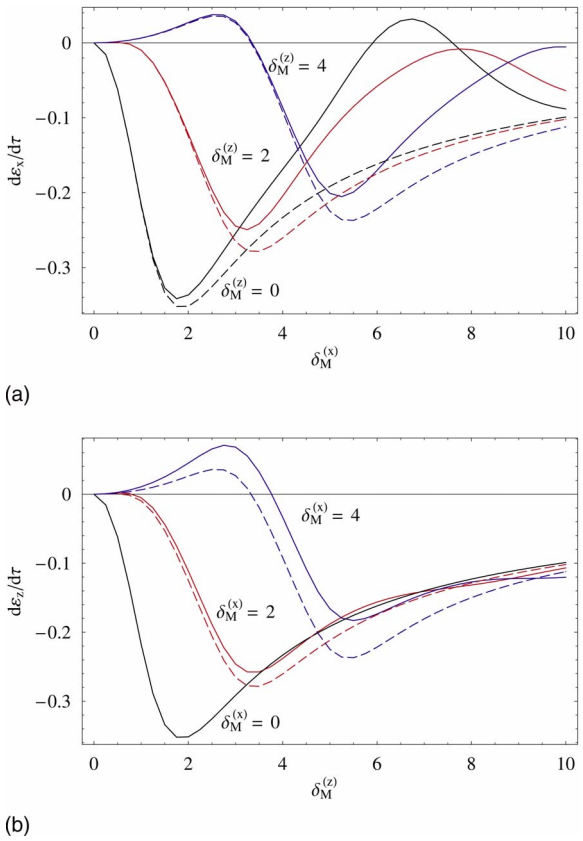

FIG. 8. (Color online) Predicted cooling rates for (a) a transverse mode in the presence of an excited z mode and (b) the z mode in the presence of a single excited transverse mode at $\delta = -1$. Dashed lines assume that the trapping potential has no associated micromotion, as described by Eq. (21). In this case, the cooling rates are of course identical for the two cases. The solid lines assume the transverse confinement to be provided by a rf quadrupole potential with a frequency $\tilde{\Omega} = 6$, as described by Eq. (24). For both situations, the cooling rate is plotted with the spectator mode having a motional energy of $\delta_M = \{0,\ 2,\ \text{and}\ 4\}$. The plots are based on the weak-binding model, and thus assume secular frequencies to be small compared to the linewidth. Note that the thermalization and equilibration effect discussed in the text is clearly observed for both cases. The dot in (a) indicates the stable point discussed in the text.

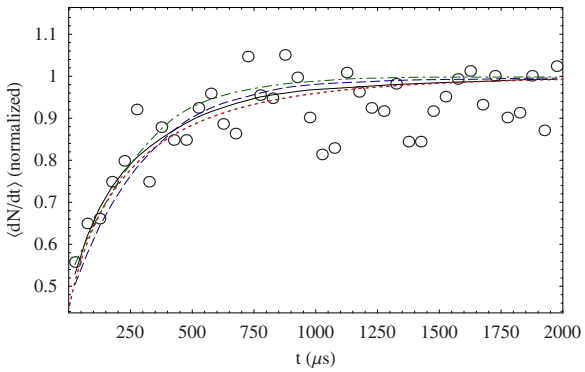

FIG. 9. (Color online) Averaged fluorescence vs time as predicted by Monte Carlo simulations for best fits to the data presented in Fig. 4 for different models of the frequency dependence of the anomalous heating rate. The solid line assumes transverse modes to be unaffected by the heating. For the dashed and dash-dotted lines, we assume heating to be proportional to $\omega^{-1.4}$ and independent of ω, respectively. The fitted value of the initial z mode temperature for the three cases is 3.9, 3.7, and 1.4 K, respectively. Assuming the transverse modes to be unaffected by heating (solid) should be very well approximated by the best fit to the 1D model (dotted), as also plotted in Fig. 4.

modes. This would, however, reduce the efficiency of cooling of the transverse modes [11].

C. Departures from the weak-binding, low-saturation limit

In most experimental situations, we will not strictly satisfy the requirements of low saturation or weak binding. In particular, for the trap referenced in Fig. 4 the secular frequencies of the transverse modes are approximately equal to half the 41.4 MHz linewidth of the Doppler cooling transition, making the weak-binding assumption only approximate. Also, the illustrated data were obtained at a saturation parameter of 0.9, outside the validity region of the line-profile model that accounts for rf micromotion (24). To validate our claim that the fluorescence signal predicted by the 1D model is a good approximation if the heating rate is assumed to be a strongly decreasing function of ω, we performed a numerical Monte Carlo simulation of the fluorescence, based on integrating the optical Bloch equations through a large number of cooling trajectories. For each trajectory, we propagate the density matrix ρ of the ion's internal state according to the master equation

$$\frac{d\rho}{dt} = \frac{i}{\hbar}[\rho, H^{(c)}(\boldsymbol{x},t)] + 2L\rho L^{\dagger} - \{L^{\dagger}L, \rho\}, \tag{25}$$

where $L \equiv |g\rangle\langle e|\sqrt{\Gamma/2}$ is the Lindblad operator for excited state decay and $\boldsymbol{x}(t) = \bar{\boldsymbol{x}}(t) + \boldsymbol{a}(\bar{\boldsymbol{x}}(t))\cos(\Omega t)$ for the $\bar{\boldsymbol{x}}$ and $\boldsymbol{a}$ introduced above. Coupling to the motional state is modeled by the average light force $m\ddot{\bar{\boldsymbol{x}}} = \hbar\boldsymbol{k}\Gamma\rho_{ee}(t)$. This model assumes neither that the atoms are weakly bound nor that the cooling beam intensity is low, but does neglect recoil heating.

Figure 9 shows the result of fitting simulations with different assumptions for the frequency dependence of the heating to the data set presented in Fig. 4. We find that, if we assume the transverse modes are not heated, we obtain a temperature estimate of 3.9 K, in agreement with the result of fitting the 1D model to the data, as illustrated by Fig. 4. The z mode temperature of 3.7 K estimated from the $\omega^{-1.4}$ model found in Ref. [20] is close to, and slightly smaller than, this value, and agrees with the temperature estimate of 3.4 ± 0.3 K based on extrapolating heating rates measured with the Raman sideband technique for the same trap configuration. This particular form of the frequency dependence of the heating rate was observed for the same trap when the Raman sideband technique [20] was used, and similar frequency dependencies have been observed in other geometries [16,18]. If we instead assume an ω^{-1} dependence of the heating, the results change only slightly.

Our main conclusions from the simulation results are that the primary effect of the presence of weakly heated spectator modes will be to slow down cooling due to thermalization. If $\omega^{-1.4}$ heating of the transverse modes is assumed, the 1D model will somewhat overestimate the motional temperature of the axial mode.

VII. MODIFIED EXPERIMENTAL PROTOCOLS

We consider two modifications to the experimental protocol to reduce the total measurement time. Both are motivated by the fact that the size of the signal from a given amount of heating increases with increased initial energy.

One approach would be to coherently add a known amount of energy to the z mode at the start of the heating period. If the added energy is enough to bring the atom into the slow-cooling regime, this will increase the signal change due to a given amount of additional heating, as illustrated in Fig. 10.

Alternatively, parametric amplification [30–32] could be employed after the heating cycle to modify the thermal distribution. Parametric amplification can be implemented by modulating the z trap potential at $2\omega_z$, and leads to amplification of one quadrature of the motion while damping the other quadrature. For a low value of $\bar{\varepsilon}$, parametric amplification would increase the fraction of experiments in which the atom is in the slow-cooling regime at the beginning of the cooling process, thus increasing the signal for a given heating period, as illustrated in Fig. 11.

The performance of either of the modified protocols outlined in this section will be determined by the uncertainty of the implementation parameters.

VIII. CONCLUSION

In conclusion, we have shown that the motional energy of a trapped atom or ion can be estimated from the temporal changes in fluorescence observed when Doppler cooling is applied. Specifically, the initial energy can be estimated by fitting Eq. (17), where the mean initial motional energy is the only free variable, to the observed fluorescence. Our analysis assumes the oscillation frequency of the atoms is much smaller than the linewidth of the optical transition used for

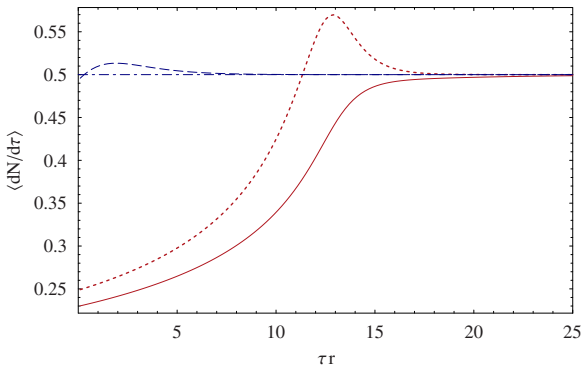

FIG. 10. (Color online) Improving the sensitivity of the temperature measurement by deliberate excitation. The dotted line shows the average scattering rate (17) as a function of time for an atom that was deliberately excited to a motional energy exactly equal to $\varepsilon_0=4/r$, so that $P_0(\varepsilon)=\delta_{\mathrm{Dirac}}(\varepsilon-\varepsilon_0)$. The solid line shows the scattering rate as a function of time for an atom which has first been deliberately excited to a motional energy of $\varepsilon_0=4/r$ and then allowed to heat for a duration that added an average thermal energy of $\bar{\varepsilon}=0.75/r$. For comparison, the dashed (dash-dotted) line shows the signal for an atom experiencing the same (no) heating period without any initial excitation, i.e., with $\bar{\varepsilon}=0.75/r$ ($\bar{\varepsilon}=0$). In all cases, $\delta=-1$. With initial (deliberate) excitation, the change in fluorescence rate due to the heating is seen to be larger.

Doppler cooling and the motional energy at the start of the cooling is thermal.

Compared to Raman sideband transition methods for heating rate measurements, this method is simpler to implement experimentally but requires longer measurement duration for traps with low heating rates. On the other hand, for high heating rates, where sideband cooling is inefficient, this may be the method of choice. We have shown that, in the typical situation, where the time for heating dominates, the total measurement time decreases with decreasing laser intensity, decreasing laser detuning, and increased heating period duration. We have compared the trade-off between these parameters [Fig. 5 and Eq. (20)]. Finally, we indicate (Sec. VII) that the total measurement time can be reduced by adding additional energy to more quickly bring the ion into the low-fluorescence regime.

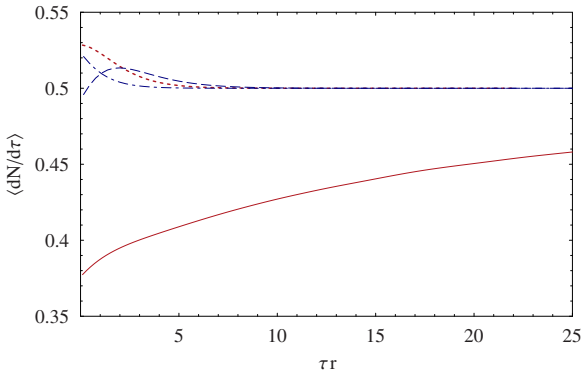

FIG. 11. (Color online) Improving the sensitivity of the temperature measurement by parametric amplification. The solid (dotted) line shows the average scattering rate vs time during the recooling of an atom which has been allowed to heat to $\bar{\varepsilon}=0.75/r$ ($0.05/r$) and then subjected to parametric amplification by a factor of 3. For comparison, the dashed and dash-dotted lines show the average scattering rate for the same heating ($\bar{\varepsilon}=0.75/r$ and $0.05/r$, respectively), but without parametric amplification. In all cases, $\delta=-1$.

By comparison with various models of three-dimensional Doppler cooling, we have established that under typical experimental conditions the effects of the high-frequency modes are small, and that they will lead to temperature estimates that are somewhat higher than the actual temperature of the low-frequency mode.

ACKNOWLEDGMENTS

This work was supported by NIST and the Disruptive Technology Office (DTO) under Contract No. 712868. J.H.W. acknowledges support from The Danish Research Agency. R.J.E. acknowledges support from the National Research Council. S.S. acknowledges support from the Carlsberg Foundation. J.P.H. acknowledges support from the Lindemann Foundation. We thank J. J. Bollinger and C. Ospelkaus for comments on the manuscript.

APPENDIX A: INTEGRALS

The integrals appearing in Eqs. (9), (11), and (21) are all convolution integrals of elements with analytical Fourier transforms and can thus be easily evaluated in Fourier space. For the 1D integrals, the inverse Fourier transform can also be performed analytically. Here we present a more direct approach to evaluating the 1D integrals.

For $a,b\in\mathbb{R}$ we define $Z(a,b)$ as

$$Z\equiv\int_0^{2\pi}\frac{1}{\sin(\phi)-z}\frac{d\phi}{2\pi}=-\frac{1}{z}\sqrt{\frac{z^2}{z^2-1}},\tag{A1}$$

where $z=(a+i)/b$. Noting that

$$\frac{1}{x-z}=b\frac{1}{1+(a-bx)^2}[(bx-a)+i],\tag{A2}$$

we find that, according to Eq. (A1),

$$\int_0^{2\pi}\frac{b\sin(\phi)}{1+[a-b\sin(\phi)]^2}\frac{d\phi}{2\pi}=\frac{1}{b}[\mathrm{Re}(Z)+a\,\mathrm{Im}(Z)],$$

$$\int_0^{2\pi}\frac{1}{1+[a-b\sin(\phi)]^2}\frac{d\phi}{2\pi}=\frac{1}{b}\mathrm{Im}(Z).$$

Taking the branch cut discontinuity for $\sqrt{\cdot}$ to be along the negative real axis, we have for $b>0$ that $\sqrt{(-iz)^2}=-iz$, so that

$$Z(a,b)=\frac{ib}{\sqrt{b^2-(a+i)^2}},\quad b>0.\tag{A3}$$

APPENDIX B: NUMERICAL CALCULATION OF THE AVERAGED SCATTERING RATE

In this section we present an efficient numerical method for evaluating the averaged scattering rate given by Eq. (17).

Introducing $\varepsilon_n = \Xi(\varepsilon_0, n\Delta\tau)$, for $n=0,1,\ldots$, we note that $\Xi(\varepsilon_m, n\Delta\tau) = \varepsilon_{m+n}$. The values of ε_n are the energies along a single cooling trajectory. If the scattering rate can be considered constant on time scales of $\Delta\tau$,

$$\frac{dN}{d\tau}[\Xi(\varepsilon_0,\tau)] \approx R_n, \quad \tau \in [(n-1)\Delta\tau, n\Delta\tau], \tag{B1}$$

we find that the thermally averaged scattering rate, as given by Eq. (17), averaged over the same intervals can be approximated by

$$\bar{R}_n \approx \sum_{m=0}^{\infty} R_{m+n} \int_{\varepsilon_{m+1}}^{\varepsilon_m} P_0(\varepsilon')d\varepsilon'. \tag{B2}$$

Since the values of the R_n are independent of P_0, $\bar{R}_n$ is easily calculated for different P_0 by list convolution.

For the Maxwell-Boltzmann distribution, a numerically stable form of the weight factors appearing in (B2) is

$$\int_{\varepsilon-\Delta\varepsilon/2}^{\varepsilon+\Delta\varepsilon/2} e^{-\varepsilon'/\bar{\varepsilon}} \frac{d\varepsilon'}{\bar{\varepsilon}} = 2e^{-\varepsilon/\bar{\varepsilon}} \sinh\left(\frac{\Delta\varepsilon}{2\bar{\varepsilon}}\right).$$

[1] F. Diedrich, J. C. Bergquist, W. M. Itano, and D. J. Wineland, Phys. Rev. Lett. **62**, 403 (1989).
[2] C. Monroe, D. M. Meekhof, B. E. King, S. R. Jefferts, W. M. Itano, D. J. Wineland, and P. Gould, Phys. Rev. Lett. **75**, 4011 (1995).
[3] H. Perrin, A. Kuhn, I. Bouchoule, and C. Salomon, Europhys. Lett. **42**, 395 (1998).
[4] D. Leibfried, T. Pfau, and C. Monroe, Phys. Today **51** (4), 22 (1998).
[5] D. J. Wineland and W. M. Itano, Phys. Rev. A **20**, 1521 (1979).
[6] D. J. Wineland, R. E. Drullinger, and F. L. Walls, Phys. Rev. Lett. **40**, 1639 (1978).
[7] W. Neuhauser, M. Hohenstatt, P. Toschek, and H. Dehmelt, Phys. Rev. Lett. **41**, 233 (1978).
[8] J. Javanainen and S. Stenholm, Appl. Phys. **21**, 283 (1980).
[9] J. Javanainen and S. Stenholm, Appl. Phys. **24**, 71 (1981).
[10] J. Javanainen and S. Stenholm, Appl. Phys. **24**, 151 (1981).
[11] W. M. Itano and D. J. Wineland, Phys. Rev. A **25**, 35 (1982).
[12] R. Blümel, C. Kappler, W. Quint, and H. Walther, Phys. Rev. A **40**, 808 (1989).
[13] R. G. DeVoe, J. Hoffnagle, and R. G. Brewer, Phys. Rev. A **39**, 4362 (1989).
[14] J. I. Cirac, L. J. Garay, R. Blatt, A. S. Parkins, and P. Zoller, Phys. Rev. A **49**, 421 (1994).
[15] E. Peik, J. Abel, T. Becker, J. von Zanthier, and H. Walther, Phys. Rev. A **60**, 439 (1999).
[16] Q. A. Turchette *et al.*, Phys. Rev. A **61**, 063418 (2000).
[17] S. Seidelin *et al.*, Phys. Rev. Lett. **96**, 253003 (2006).
[18] L. Deslauriers, S. Olmschenk, D. Stick, W. K. Hensinger, J. Sterk, and C. Monroe, Phys. Rev. Lett. **97**, 103007 (2006).
[19] C. E. Pearson, D. R. Leibrandt, W. S. Bakr, W. J. Mallard, K. R. Brown, and I. L. Chuang, Phys. Rev. A **73**, 032307 (2006).
[20] R. J. Epstein *et al.*, Phys. Rev. A **76**, 033411 (2007).
[21] H. Walther, Adv. At., Mol. Opt. Phys. **31**, 137 (1993).
[22] D. J. Wineland, C. R. Monroe, W. M. Itano, D. Leibfried, B. E. King, and D. Meekhof, J. Res. Natl. Inst. Stand. **103**, 259 (1998).
[23] D. J. Wineland, in *Quantum Entanglement and Information Processing*, Proceedings of the Les Houches Summer School of Theoretical Physics, LXXIX, 2003, edited by D. Estève, J.-M. Raimond, and J. Dalibard (Elsevier, Amsterdam, 2004), pp. 261–293.
[24] R. Loudon, *The Quantum Theory of Light* (Clarendon, Oxford, 1973).
[25] A. L. Wells and R. J. Cook, Phys. Rev. A **41**, 3916 (1990).
[26] I. Press and H. William, *Numerical Recipes in Pascal* (Cambridge University Press, Cambridge, U.K., 1989).
[27] T. Sauter, H. Gilhaus, W. Neuhauser, R. Blatt, and P. E. Toschek, Europhys. Lett. **7**, 317 (1988).
[28] T. Sauter, H. Gilhaus, I. Siemers, R. Blatt, W. Neuhauser, and P. E. Toschek, Z. Phys. D **10**, 153 (1988).
[29] D. J. Berkeland, J. D. Miller, J. C. Bergquist, W. M. Itano, and D. J. Wineland, J. Appl. Phys. **83**, 5025 (1998).
[30] H. G. Dehmelt and F. L. Walls, Phys. Rev. Lett. **21**, 127 (1968).
[31] C. M. Caves, Phys. Rev. D **26**, 1817 (1982).
[32] D. J. Heinzen and D. J. Wineland, Phys. Rev. A **42**, 2977 (1990).